Wind and Structures, *Vol. 24, No. 1 (2017) 25-41*
DOI: https://doi.org/10.12989/was.2017.24.1.025

Wind pressures on different roof shapes of a finite height circular cylinder

Y. Ozmen*[1] and E. Aksu[2]

[1]*Department of Mechanical Engineering, Karadeniz Technical University, Trabzon 61080, Turkey*
[2]*Naval Architecture and Marine Engineering, Karadeniz Technical University, Trabzon 61080, Turkey*

(Received January 13, 2016, Revised November 3, 2016, Accepted November 5, 2016)

Abstract. The effects of finite cylinder free end shape on the mean and fluctuating wind pressures were investigated experimentally and numerically by using three different roof shapes: flat, conical and hemispherical. The pressure distributions on the roofs and the side walls of the finite cylinders partially immersed in a simulated atmospheric boundary layer have been obtained for three different roof shapes. Realizable *k-ε* turbulence model was used for numerical simulations. Change in roof shapes has caused significant differences on the pressure distributions. When compared the pressure distributions on the different roofs, it is seen from the results that hemispherical roof has the most critical pressure field among the others. It is found a good agreement between numerical and experimental results.

Keywords: finite cylinder; circular flat roof; conical roof; hemispherical roof; suction pressure; realizable k-ε turbulence model

1. Introduction

The roofs of finite cylindrical buildings such as tall buildings, gymnasiums and hangars are built in different geometries due to their attractive architectural shapes. Many high-rise buildings are structured as a finite cylinder with a free end. Pressure distribution on the free end of finite cylinder has been affected from the roof shape. For this reason, the evaluation of the pressure distribution on the different roof geometries is very important for wind engineering applications.

There are some studies about the pressure distributions on flat, conical and hemispherical roofs of cylindrical buildings in literature. Purdy, Maher *et al.* (1967) obtained pressure distributions on the cylinders with a flat roof. Farivar (1981) investigated the effect of finite cylinder free end on the mean pressure, pressure fluctuations and drag force. Okamoto and Sunabashiri (1992) found that the wake behind finite cylinder of small aspect ratio is symmetric. Kareem and Cheng (1999) experimentally obtained mean and fluctuating pressure distributions on a cylinder of finite height in simulated turbulent boundary layer flows at subcritical Reynolds numbers. Uematsu, Watanabe *et al.* (1999) presented the results of a wind pressure measurement in a wind tunnel as well as of a dynamic-response analysis of a circular flat roof. The results indicated that a gust loading factor approach can be applied to the evaluation of the design wind loads for the structural frame of

*Corresponding author, Associate professor, E-mail: yozmen@ktu.edu.tr

http://www.techno-press.org/?journal=was&subpage=8 ISSN: 1226-6116 (Print), 1598-6225 (Online)

circular flat roofs.

Kitagawa, Fujino *et al.* (2002) measured wind pressure acting on a rigid circular tower and studied the characteristics of the pressures originated tip-associated vortices. Park and Lee (2002) investigated the wake structure behind an isolated finite cylinder embedded in various atmospheric boundary layers with the measurements of wake velocity and mean pressure distribution on the cylinder surfaces. Park and Lee (2003) examined the effect of the gap distance between two finite cylinders embedded in atmospheric boundary layer on the flow characteristics of the near-wake and elucidated the flow structure near the finite cylinder free end in detail. Pattenden, Turnock *et al.* (2005) studied the flow over a finite-height cylinder of aspect ratio 1 by means of surface flow visualization, particle image velocimetry and surface pressure measurements. Sumner and Heseltine (2008) studied the wake of a finite circular cylinder mounted normal to a ground plane in a low-speed wind tunnel experimentally. Uematsu, Moteki *et al.* (2008) investigated the characteristics of wind pressures acting on circular flat roofs with a wind tunnel experiment. Hain, Köhler *et al.* (2008) performed tomographic and time resolved PIV measurements to examine the 3D flow topology and the flow dynamic above the upper surface of a low-aspect ratio cylinder. Dobriloff and Nitshe (2009) conducted the surface pressure and wall shear stress measurements on a finite wall mounted circular cylinder and in the vicinity of cylinder.

Sabransky and Melbourne (1987) obtained wind pressure distributions on the circular cylindrical walls and conical roofs of typical grain storage silos. Macdonald, Kwok *et al.* (1988) obtained wind pressures on tanks with a conical roof. A comprehensive study of the aerodynamic pressure distribution on hemispherical domes including the determination of the mean, standard deviation, minimum and maximum and area average pressure coefficients is conducted by Taylor (1991). Hongo (1995) made a detailed measurements of wind pressures on spherical domes with rise/span ratios ranging from zero (flat roof) to 0.5 (hemisphere) in a wind tunnel. Maher (1996) performed a wind tunnel study on cylindrical tanks with spherical roofs. Leder (2003) measured the wake behind a cylinder of aspect ratio 2, with two different end shapes flat and hemispherical and showed that change in end shape cause change in vorticity. Blackmore, Tsorki *et al.* (2004) investigated the wind loads on the cylindrical and curved roofed buildings to provide architects and designers with an alternative to regular rectangular building forms. Park and Lee (2004) studied flow structure near the various free ends of the finite cylinder immersed in an atmospheric boundary layer. They systematically varied the free-end corner shape and carried out flow analysis using the PIV technique, flow visualization and hot-wire anemometry. Portela and Godoy (2005a) conducted wind tunnel experiments using finite cylindrical model with a conical roof and obtained pressure distributions due to wind on the cylindrical part and on the roof. They concluded that conical roofs are responsible for an increase in pressures on the central part of the roof. Portela and Godoy (2005b) obtained pressure distributions on the cylindrical steel tanks with a dome roof. They noted that the details of the geometric transition between the cylindrical body and the roof are crucial in the evaluation of pressures on the roof, since this transition changes the main features of the flow separation. Li, Tamura *et al.* (2006) obtained wind pressure distributions on cylindrical shells considering different aspect ratios in the wind tunnel models. Cheng and Fu (2010) performed a series of pressure measurements on a hemispherical dome to investigate Reynolds number effects on characteristics of wind loads. Wang and Lee (2015) conducted a wind tunnel study to measure internal and external pressures on a low-rise building model with different openings on its roof corners. They noted that the length of the front edge of the roof affects the development of conical vortices on the corner. Mooneghi, Irwin *et al.* (2016) performed large scale experiments to investigate the wind loading on concrete roof pavers on the flat roof of a low-rise

building. They developed a simplified guideline for design of loose-laid roof pavers against wind uplift.

Fröhlich and Rodi (2004) investigated flow field around a surface mounted circular cylinder of height 2.5 times the diameter by using large eddy simulations method. They showed that the results obtained from numerical model are in fairly good agreement with measurements. Afgan, Moulinec *et al.* (2007) numerically investigated flow structure around wall mounted circular cylinders of finite height for different aspect ratios with large eddy simulation (LES) and then compared to experimental results. They found that pressure coefficient profile at mid-height of finite cylinder is significantly different from that of an infinite cylinder. Air flow field around a surface-mounted hemisphere of a fixed height for two different turbulent boundary layers are investigated experimentally and numerically by Tavakol, Yaghoibu *et al.* (2010). Faghih and Bahadori (2010) determined the air pressure distribution over domed roofs employing 3D RNG k-ε turbulence model. Krajnovic (2011) investigated the flow around a tall fine cylinder using LES. The flow resulting from the LES was used to present a detailed picture of both the instantaneous and the time-averaged flow. Turbulent flow over a wall mounted finite cylinder with free end was simulated with LES by Javadi and Kinai (2014).

Conical and spherical roofed buildings are increasingly used in the modern built environment because they offer aerodynamically efficient shapes and provide architects and designers with an alternative to regular rectangular building forms. The determination of wind induced loads on flat, conical and spherical roofs of finite cylinders is essential to the design of these roofs knowledge of the effects of architectural details on these loads is also of interest. It is of importance to define both the location and magnitude of these suctions. There is little information available on the wind loads on these kinds of roofs. The purpose of this study is to examine the distributions of wind loads on flat, conical and spherical roofs of finite cylinders and reveal the changes in pressure distribution on these roofs. For this reason, three different roof types were introduced to examine their influence on the distribution of pressure field.

2. Experimental details

The experiments were carried out in a low speed, open circuit wind tunnel with a test section of 457 mm high, 457 mm wide and 2450 mm long. The combination of barrier, vortex generators and roughness elements at the entrance to the test section was used to simulate atmospheric boundary layer (power-law exponent, n=0.2) over a city suburb. Cylindrical models with different roofs were constructed to a geometric scale of 1:50. A turbulent boundary layer of 150 mm thickness was obtained at the free stream velocity of 15 m/s, giving a Reynolds number based on cylinder diameter of Re=100000. A schematic diagram of the wind tunnel test-section and the measurement system is given in Fig. 1. δ and H represent the boundary layer thickness and characteristic height of model, respectively. A smoke-wire technique is used to visualize the flow structure around models. A 0.2 mm diameter stainless steel wire is vertically located at the entrance of test section. Before each test the smoke-wire was coated by paraffin oil and then heated by Joule effect of DC current. The flow pattern visualized is photographed successively by a video camera. Flow visualization is performed at Re=20000 since this technique is limited to the small Reynolds numbers.

The mean and fluctuating surface pressure measurements were conducted with a measurement chain system consisting of the components of signal conditional module, Setra 239 pressure

transducer, A/D converter, package and computer. The output of the pressure transducer was fed through a signal conditioning unit before being digitized and recorded. The signals from the transducer are sampled at a rate of 1000 samples per second for a period of 16 s and data were low-pass filtered at 300 Hz. Measurements have been performed at the spacing of 15° wind angle along the mid-axis of the model. The mean and fluctuating velocity measurements at the reference boundary layer were performed with TSI IFA 100 constant-temperature anemometer and TSI model 1211 hot-film probe.

The cylindrical models having different roof shapes and the distribution of the pressure measurement taps on their surfaces are shown in Fig. 2. The models used in this study were made of polyvinyl chloride. The dimensions of cylindrical part of the models were H=150 mm, D=100 mm. H represent model height and D is the model diameter for cylindrical part. Heights of conical and hemispherical roofs are the same as 50 mm. Roof and wall pressures were measured for cylindrical building models having flat, conical and hemispherical roof shapes. To obtain the surface pressure distributions, 16 pressure taps of 0.8 mm inner diameters were placed on the roof and the side wall of cylinder and the models were rotated from 0° to 180° in 15° increments in a counter clockwise direction (θ) as incoming flow. A scanning valve was used to supply linkage from pressure taps to pressure transducer. All pressure taps were connected to a scanning valve using 60 cm lengths of vinyl tubing with 1 mm inside diameter. The pressure difference between the local surface pressure (P) and the static pressure (P_o) was divided by the reference dynamic pressure at a equivalent height to give pressure coefficient C_p expressed as $C_p=(P-P_o)/0.5\rho U_o^2$, where U_o is the free-stream velocity and ρ is the air density. Ambient temperature and atmospheric pressure were continuously recorded during the experiments to identify changes in the air density which could affect the local pressures measured in the wind tunnel. The blockage ratio defined as the ratio of the projected model area to the cross-sectional area of test section is 9%. Correction for the effect of the wind tunnel blockage was made in this study. West and Apelt (1982) found that the surface pressure distribution of a circular cylinder varies only slightly with respect to the blockage ratio of the model. The uncertainties of mean and fluctuating velocity measurements are found as ± % 2 and ± % 4, respectively. The uncertainties of mean and fluctuating pressure measurements are ± % 3 and ± % 4.5, respectively (Holman 1994). The experimental results were reproducible within these uncertainty ranges.

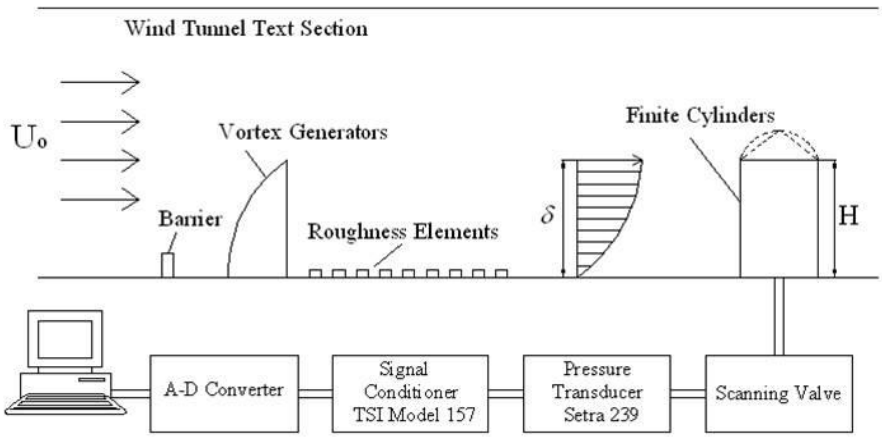

Fig. 1 Wind tunnel test section and pressure measurement system

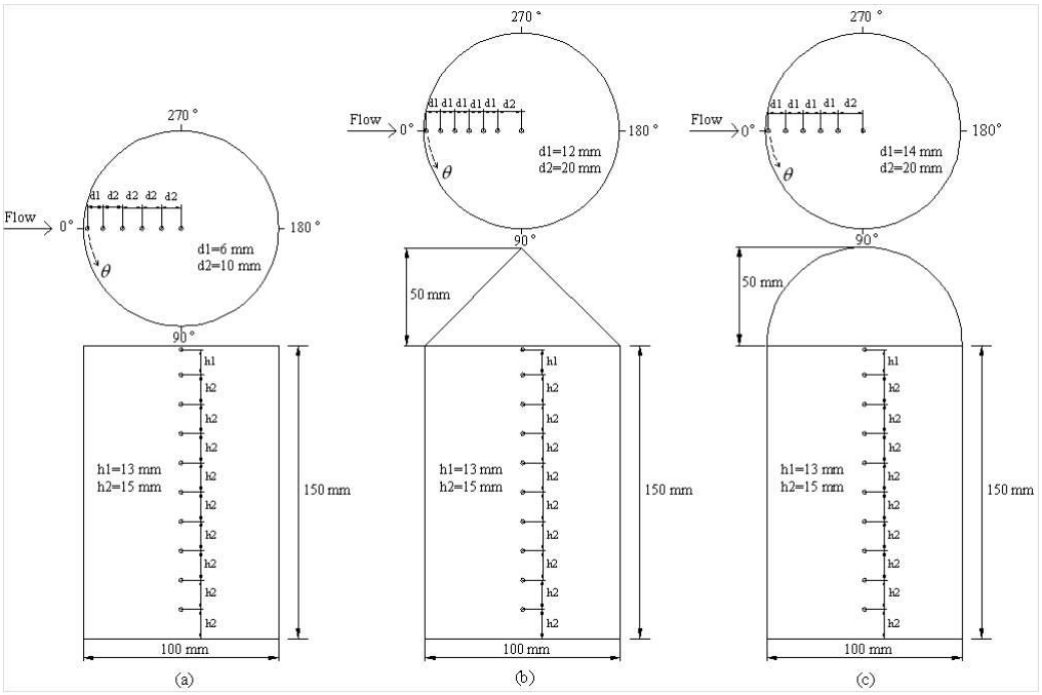

Fig. 2 Dimensions of model geometries (a) cylindirical model with a flat roof, (b) cylindirical model with a conical roof and (c) cylindirical model with a hemispherical roof

3. Numerical study

3.1 Mathematical model

In the present study, it is assumed that the air flow is turbulent, steady-state and Newtonian with temperature-dependent fluid properties. A numerical solution of the mean flow field requires resolving the Reynolds averaged Navier-Stokes equations. These equations for three-dimensional, incompressible and continuity flow in Cartesian tensor form can be written as given below,

mass continuity

$$\frac{\partial}{\partial x_i}(\rho u_i) = 0 \tag{1}$$

momentum

$$\frac{\partial}{\partial x_j}(\rho u_i u_j) = -\frac{\partial P}{\partial x_i} + \frac{\partial}{\partial x_j}\left[\mu\left(\frac{\partial u_i}{\partial x_j} + \frac{\partial u_j}{\partial x_i} - \frac{2}{3}\delta_{ij}\frac{\partial u_i}{\partial x_j}\right)\right] + \frac{\partial}{\partial x_j}\left(-\rho\overline{u_i' u_j'}\right) \tag{2}$$

where, the term $\left(-\rho\overline{u_i' u_j'}\right)$ is the Reynolds stress, defined as

$$-\rho\overline{u_i'u_j'} = \mu_t\left(\frac{\partial u_i}{\partial x_j}+\frac{\partial u_j}{\partial x_i}\right)-\frac{2}{3}\left(\rho k+\mu_t\frac{\partial u_i}{\partial x_i}\right)\delta_{ij} \quad (3)$$

Numerical solutions are performed by using Realizable k-ε turbulence model because of capturing the near-wall turbulence effects more accurately. This turbulence model is more responsive to the effects of rapid strain and streamlines curvature, flow separation, reattachment and recirculation. This model consists of two transport equations which solve the turbulent kinetic energy (k) and turbulent dissipation rate (ε). The transport equations are as follows

$$\frac{\partial}{\partial x_i}(\rho k u_j) = \frac{\partial}{\partial x_i}\left[\left(\mu+\frac{\mu_t}{\sigma_k}\right)\frac{\partial k}{\partial x_j}\right]+G_k+G_b-\rho\varepsilon-Y_M+S_k \quad (4)$$

$$\frac{\partial}{\partial x_j}(\rho\varepsilon u_j) = \frac{\partial}{\partial x_j}\left[\left(\mu+\frac{\mu_t}{\sigma_\varepsilon}\right)\frac{\partial \varepsilon}{\partial x_j}\right]+\rho C_1 S_\varepsilon-\rho C_2\frac{\varepsilon^2}{k+\sqrt{\nu\varepsilon}}+C_{1\varepsilon}\frac{\varepsilon}{k}C_{3\varepsilon}G_b+S_\varepsilon \quad (5)$$

where G_k is the production of turbulent kinetic energy due to the mean velocity gradients, G_b represents the generation of the turbulent kinetic energy due to buoyancy while Y_M is referred to the fluctuation rates related to the overall dissipated turbulent thermal energy. σ_k and σ_ε represent the turbulent Prandtl numbers based on k and ε, respectively; while S_k and S_ε are further generation terms. The turbulent viscosity is defined by

$$\mu_t = \rho C_\mu\frac{k^2}{\varepsilon} \quad (6)$$

The model constants for the Realizable k-ε model are given by:
$C_{1\varepsilon} = 1.44,\ C_2 = 1.9,\ \sigma_k = 1.0\ and\ \sigma_\varepsilon = 1.2.$ C_μ is no longer a constant in this model.

3.2 Flow field and boundary conditions

A schematic of computational domain is shown in Fig. 3 where the flow field, the main dimensions and the prescribed boundary conditions are specified. Only half of the models was used for simulation because of symmetry. Therefore, the boundary condition of one lateral surface is symmetrical. The boundary conditions on the models surfaces and the other lateral surfaces were considered as wall. No slip assumption used for wall shear condition. The mean velocity and turbulence profiles measured at reference boundary layer were used as velocity inlet conditions of computational domain and pressure outlet boundary conditions were assumed at outlet planes.

3.3 Numerical solution procedure

The governing equations were solved using the ANSYS-FLUENT 14, by finite volume discretization, using a segregated solver with an implicit formulation. The discretized equations for the pressure-velocity coupling were solved by using the SIMPLEC algorithm on staggered grids. SIMPLEC procedure uses modified equation for face flux correction. The use of modified correction equation accelerates convergence. Pressure was solved using standard discretization scheme. A second order discretization method was used for the other variables (momentum, turbulent kinetic energy and turbulence dissipation rate). Second order discretization scheme presents higher-order accuracy especially for complex flows involving separation. Enhancement

wall treatment was used as wall function to obtain reasonably accurate predictions near the wall. The convergence criterion for the residuals was set to $1x10^{-5}$ for all dependent variables. Vertical slices of the three dimensional meshes near the cylindrical buildings having different roof types are shown in Fig. 4. Non-uniform structured grid is used to discretize the governing equations. To ensure the attainment of grid-independent results, sensitivities of both grid numbers and grid distributions were tested for each case. The mesh used was refined for each model until negligible differences were obtained. Finally, total number of 700000 grid cells were used to obtain grid independent results for the building models.

4. Result and discussion

The mean velocity and turbulence intensity profiles of the stream wise velocity component measured at the reference boundary layer are shown in Fig. 5. It is seen that mean velocity profile in the reference boundary layer agrees well with power law of n=0.2 and the turbulence intensity near the wall reaches up to 11%.

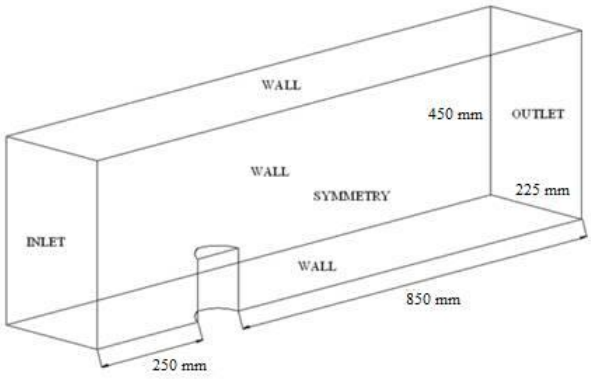

Fig. 3 Dimensions of the solution domain, and the boundary conditions

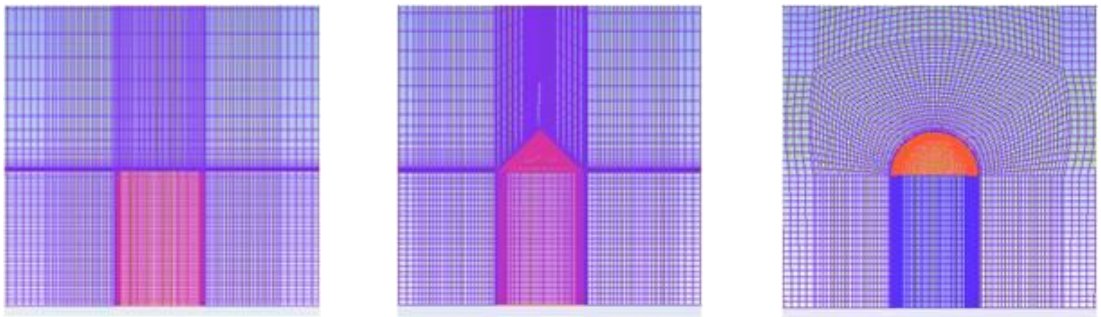

(a) (b) (c)

Fig. 4 A vertical slice of the three dimensional mesh near the cylindrical building. (a) with flat roof, (b) with conical roof and (c) with hemispherical roof

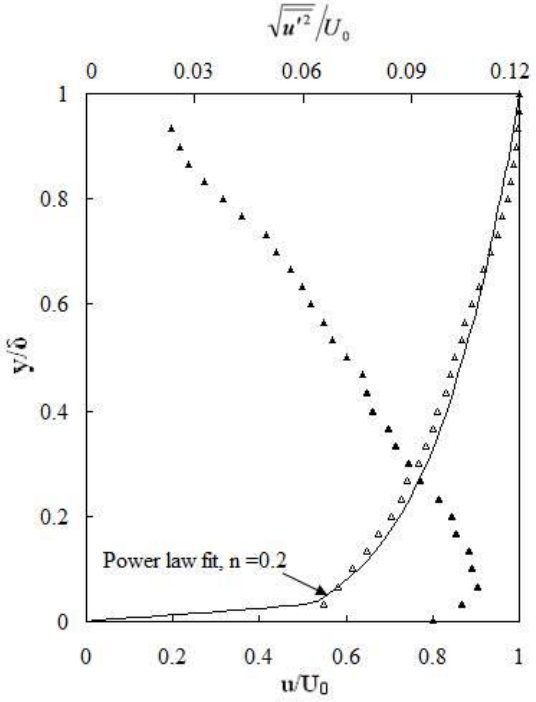

Fig. 5 Profiles of mean velocity and turbulence intensity

Flow patterns around cylindrical buildings having different roof shapes obtained with smoke-wire technique and Realizable k-ε turbulence model are given together in Fig. 6. In general, flow images obtained by numerical solutions are coherent with the photographs of flow visualization. Incoming flow to the flat roof is separated from the leading edge of the model and mixing layer is descended to the leeward edge of the model. Two reverse flow regions occur both on the flat roof and the rear of the model along the flow (Figs. 6(a) and 6(d)). For the building model having conical roof, the flow attaches to the windward roof and a recirculation region occurs behind of the model because of flow separated from tip of the conical roof. Formed and separated vortex stemmed from reverse flow are spread through the rear of the model along the flow. Complex recirculation regions are observed behind of the model because of the roof shape (Figs. 6(b) and 6(e)). For the model with hemi-spherical roof, incoming flow follows the model surface and separates from the top of the dome (Fig. 6(c) and 6(f)).

The resulting data consists of mean, maximum, minimum and root-mean-square (rms) values of the surface pressure which have been normalized by the free stream mean dynamic pressure. The variations of mean, maximum, minimum and rms values of pressure coefficients along the mid-axis of finite cylinder model having flat roof are given as comparatively with measurements of Uematsu, Moteki *et al.* (2008) and with the mean pressure coefficients computed from Realizable k-ε turbulence model in Fig. 7. Pressure distribution on the windward wall is positive due to impinging effect. Negative pressure fields occur both on the roof and leeward wall of the cylinder because of flow separated from the leading edge of the roof.

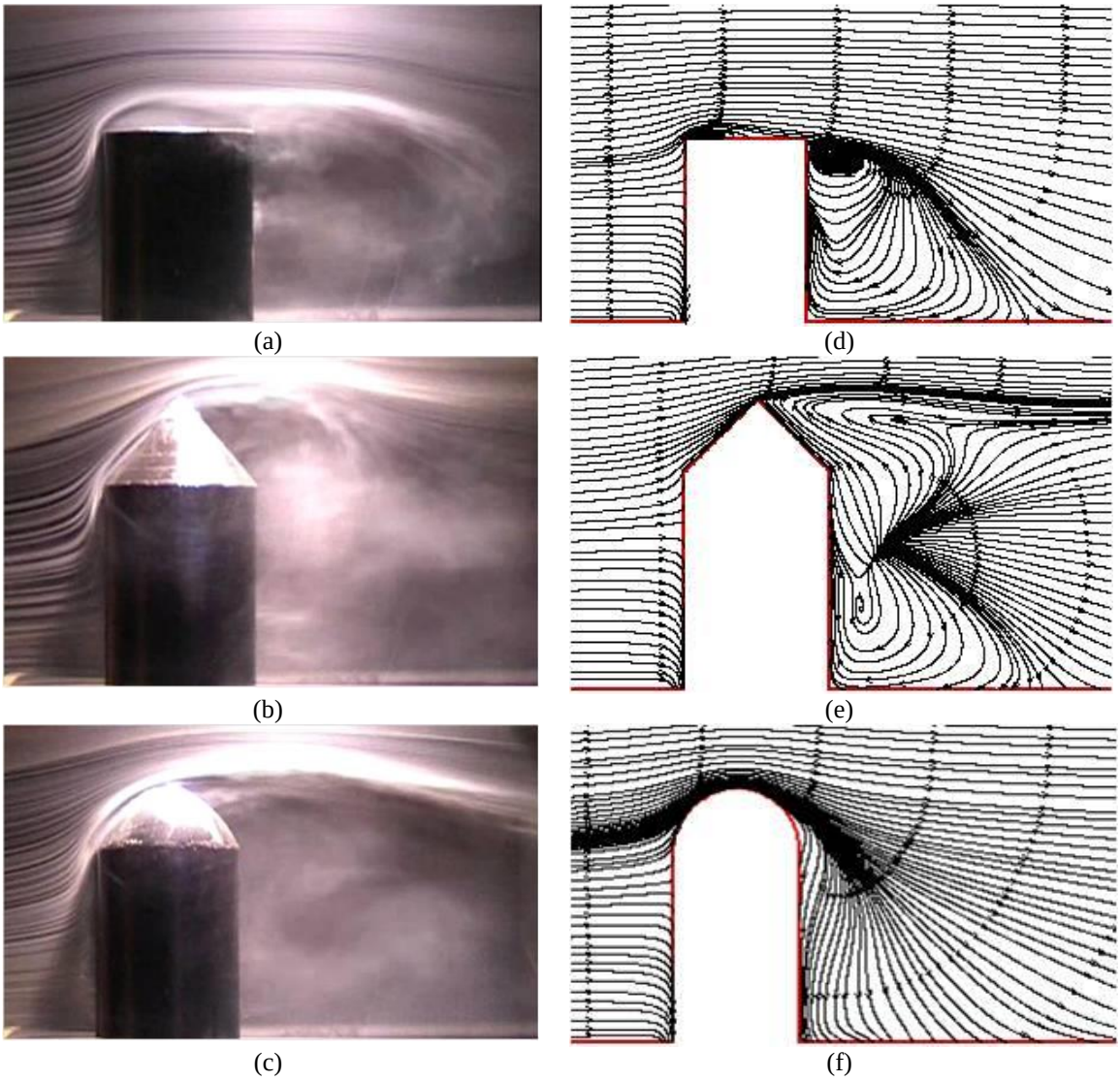

Fig. 6 Flow patterns around cylindrical buildings obtained with smoke-wire technique and Realizable k-ε turbulence model (a),(d) with flat roof, (b),(e), with conical roof, (c),(f) with hemispherical roof

The flow separated from the leading edge of circular flat roof reattaches downstream on the roof and then separates again from the leeward edge of roof. The largest negative pressures occur in separation flow region near the leading edge of the roof and are progressively reduced in magnitude in the reattachment region on the roof surface. Pressure distribution along the leeward wall is almost uniform and is under the atmospheric pressure. It is seen that there is a good accordance among the measured and computed mean pressure distributions of present study and Uematsu, Moteki *et al.* (2008) measurements. Fig. 8 show the mean and minimum pressure distributions obtained experimentally and mean pressure distribution computed with Realizable

k-ε turbulence model on the circular flat roof and cylinder surface. Fig. 8(a) shows the contours with mean pressure coefficients experimentally obtained for the flat roof of finite cylinder. There is symmetry of the pressures measured on the roof with respect to the windward meridian. It can be seen that the contour lines are roughly perpendicular to the wind direction, expect in the leeward edge of the roof where a three-dimensional effect becomes significant. Only negative values were observed on the roof, which represents suctions or pressures exerted in an outward direction. Critical negative pressures were obtained on the windward part of the roof. The highest suction was measured on the windward region of the circular roof with C_{pmean} = -1.20, as an approximate value of C_{pmean} = - 0.30 was obtained at the leeward region of the roof. Contours of mean wind pressure coefficients obtained experimentally were plotted along the circumference of the cylinder and are shown in Fig. 8(b). The positive pressure coefficients were obtained on the windward meridian, while the critical negative suctions were found at an angle near to 80° from windward. Due to the accelerating flow around the finite cylinder, the mean pressure coefficients decreases from 0.30 to -1.10 for cylinder angles of θ = 0° and 80° and the flow separates from the cylinder surface around θ = 80°.

The critical values were measured between 20% and 80% of the height of the model. The pressure coefficients measured at the leeward meridian on the top of the cylinder are similar to those measured in the leeward region of the roof. The measured pressures increase with minimum pressure coefficients of C_{pmin} = -1.50 to -0.50 on the circular flat roof from the windward region to leeward region as seen in Fig. 8(c). Critical minimum suctions measured on the circular flat roof and cylinder surface are 20% higher than mean pressure coefficients (Figs. 8(c) and 8(d)). There is a good agreement between the mean pressure distributions obtained experimentally and numerically (Fig. 8(e) and 8(f)).

Fig. 9 gives the variations of mean, maximum, minimum and rms values of pressure coefficients along the mid-axis on the conical roof of finite cylinder as comparatively with the mean pressure coefficients computed with Realizable k-ε turbulence model. Pressure coefficients take positive values on a big part of the windward roof. The negative pressure peak occurs in the separated flow region near the tip of the conical roof and are progressively reduced in magnitude on the leeward roof. Mean pressure coefficients computed numerically have the same trend with the experimental results.

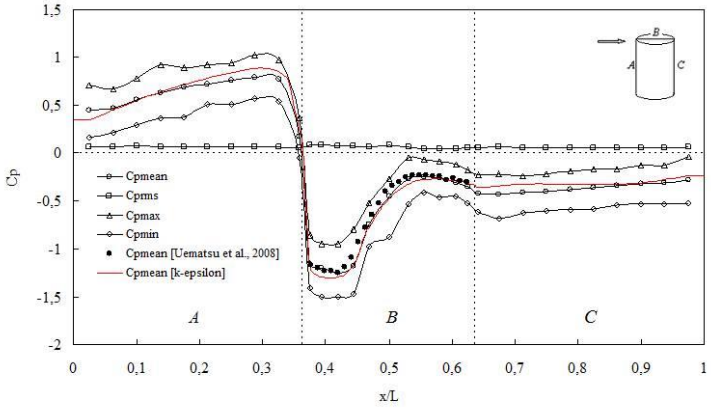

Fig. 7 Variation of pressure coefficients along the mid-axis of cylindirical model with flat roof in the flow direction

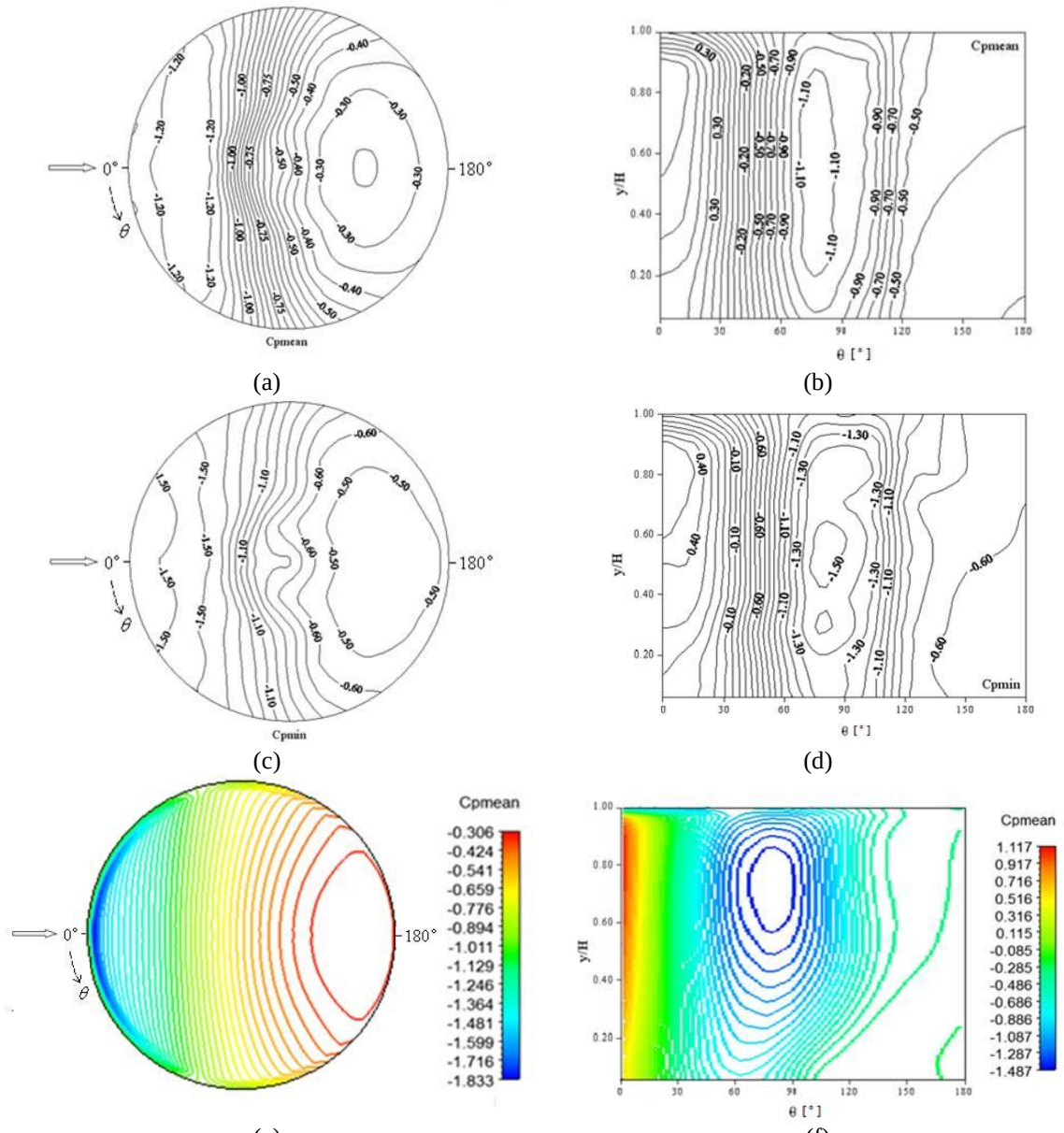

Fig. 8 Contour of mean and minimum pressure coefficients in the cylindirical model with a flat roof (a), (c), (e) roof (b), (d), (f) cylinder

Fig. 10 shows contours of mean and minimum pressure coefficients obtained experimentally and mean pressure coefficients computed with Realizable k-ε turbulence model on the conical roof respectively. There is symmetry of the pressures measured on the roof with respect to the windward meridian. Except the front part of the windward which is directly exposed to incoming flow, negative pressures were observed on the roof. Critical negative pressures were obtained on

the roof regions (at θ=90° and θ=270°) which are perpendicular to the incoming flow. At this regions, high negative values are expected due to separation of flow induced by the sudden change in the meridian between the cylinder wall and the roof surface (Portela and Godoy 2005a). The highest suction was measured on the roof regions normal to the flow with C_{pmean} = -0.80, as an approximate value of C_{pmean} = 0.10 was obtained at the windward region of the roof (Fig. 10(a)). The measured pressures increase with minimum pressure coefficients of C_{pmin} = -1.10 to -0.10 on the conical roof from the leeward region to windward region (Fig. 10(b)). Computed mean pressure distribution on the conical roof shows a good accordance with mean pressure distribution obtained experimentally (Fig. 10(c)).

Fig. 11 shows the variations of mean, maximum, minimum and rms values of pressure coefficients along the mid-axis on the hemispherical roof of finite cylinder as comparatively with the mean pressure coefficients computed with Realizable k-ε turbulence model. Except the small part of the windward roof, pressure coefficients take negative values on the hemispherical roof. The negative pressure peak occurs on the top of the dome because of the separated flow and are progressively reduced in magnitude on the leeward roof. Mean pressure coefficients obtained numerically give a good agreement with mean pressure coefficients obtained experimentally.

Contours of mean and minimum pressure coefficients obtained experimentally and mean pressure coefficients computed with Realizable k-ε turbulence model on the hemispherical roof are shown in Fig. 12. There is symmetry of the pressures measured on the roof with respect to the windward meridian. Except the small part of the windward which is directly exposed to incoming flow, negative pressures were observed on the roof. Similar to the results of conical roof, critical negative pressures were obtained on the roof regions (at θ=90° and θ=270°) which are perpendicular to the incoming flow. Portela and Godoy (2005b) and Cheng and Fu (2010) also found the values similar to those of the present study on the hemispherical roof. The highest suction was measured on the roof regions perpendicular to the incoming flow with C_{pmean} = -1.10, as an approximate value of C_{pmean} = 0.10 was obtained at the windward region of the roof (Fig. 12(a)). The measured pressures increase with minimum pressure coefficients of C_{pmin} = -1.70 to 0.20 on the conical roof from the leeward region to windward region (Fig. 12(b)). Computed mean pressure distribution on the hemispherical roof shows a good accordance with mean pressure distribution obtained experimentally (Fig. 12(c)).

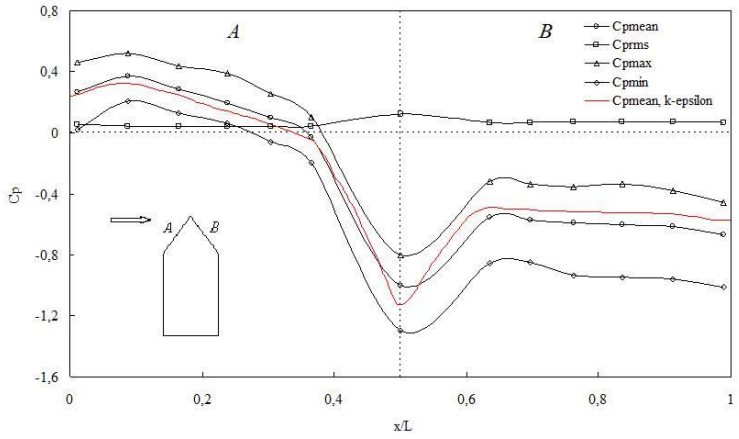

Fig. 9 Variation of pressure coefficients along the mid-axis of conical roof in the flow direction

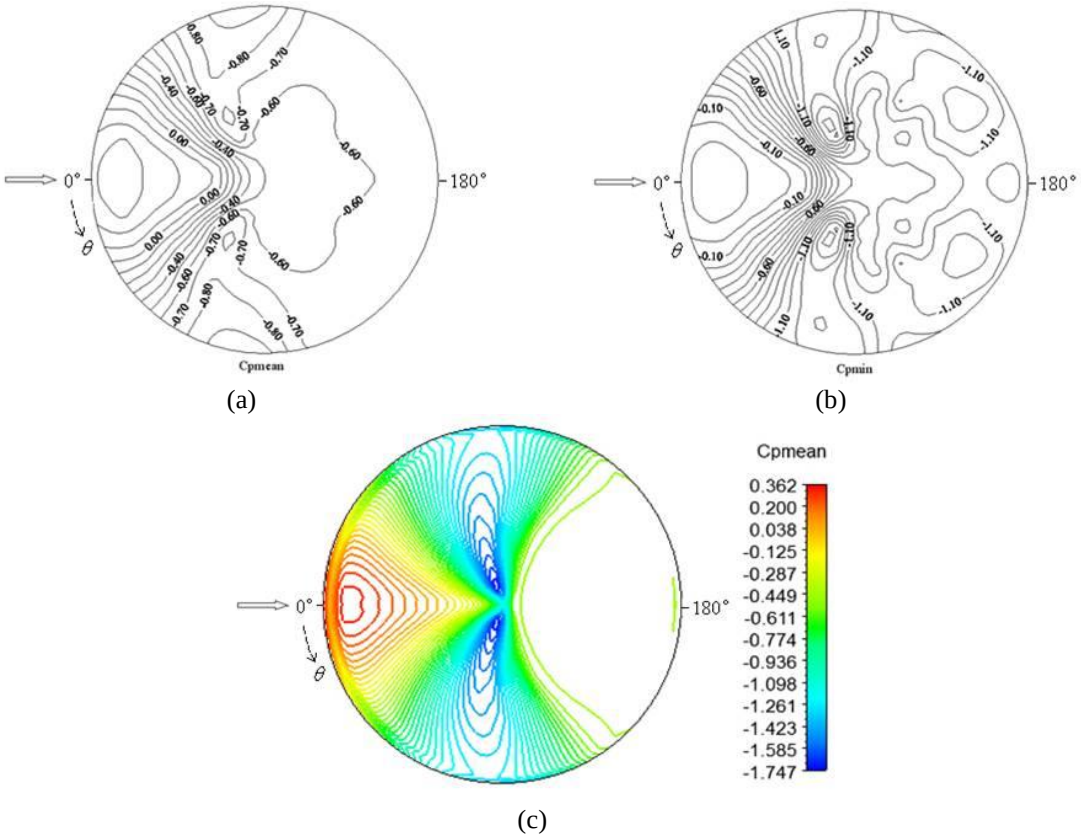

Fig. 10 Contour of pressure coefficients on conical roof (a) mean (experimental), (b) minimum (experimental) and (c) mean (numerical)

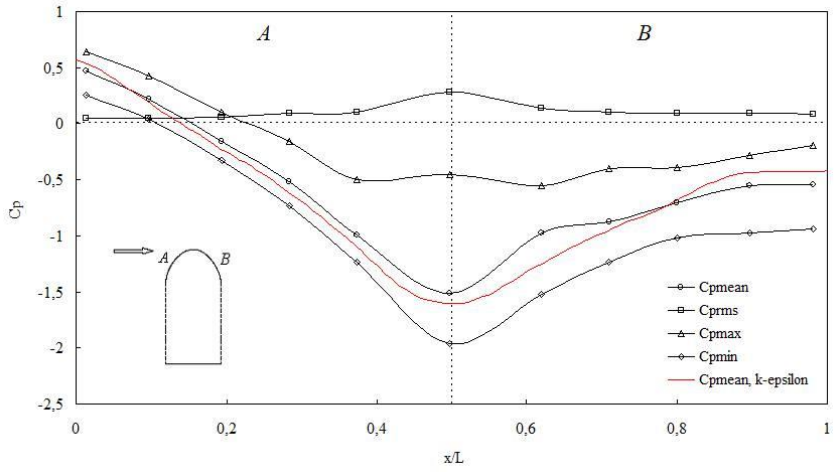

Fig. 11 Variation of pressure coefficients along the mid-axis of hemispherical roof in the flow direction

Although not shown, the pressure patterns on the cylindrical wall for conical and hemispherical roofs do not present any changes unlike the differences between pressure distributions found on the different roofs of finite cylinder.

The variations of mean and minimum pressure coefficients measured on the three different roof shapes (flat, conical and hemispherical) along the mid-axis of finite cylinder are presented in Fig. 13. Only negative pressure values were observed on the circular flat roof. Because of the flow separated from the leading edge, more critical negative pressures occur on the windward part of the flat roof.

For the conical roof, there are positive pressure coefficients on a large part of the windward roof. The negative pressure peak occurs in the separated flow region near the tip of the conical roof and are reduced in magnitude on the leeward roof. Except the small part of the windward roof, pressure coefficients take negative values on the hemispherical roof. The negative pressure peak occurs on the top of the dome because of the separated flow and are progressively reduced in magnitude on the leeward roof.

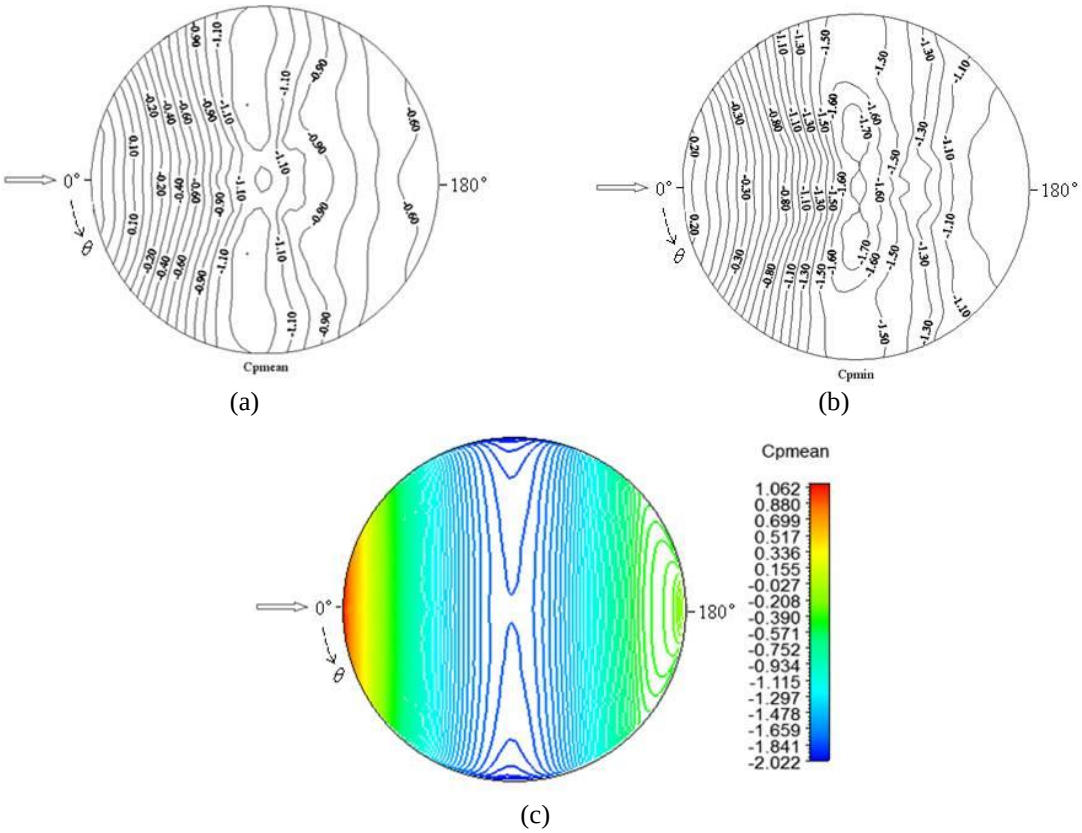

Fig. 12 Contour of pressure coefficients on semi-spherical roof (a) mean (experimental), (b) minimum (experimental) and (c) mean (numerical)

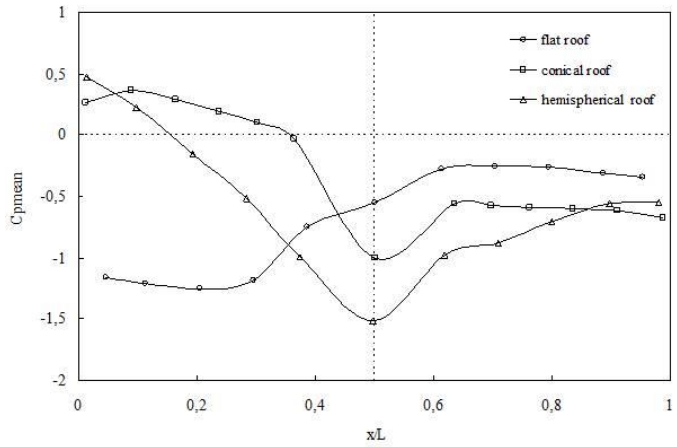

(a)

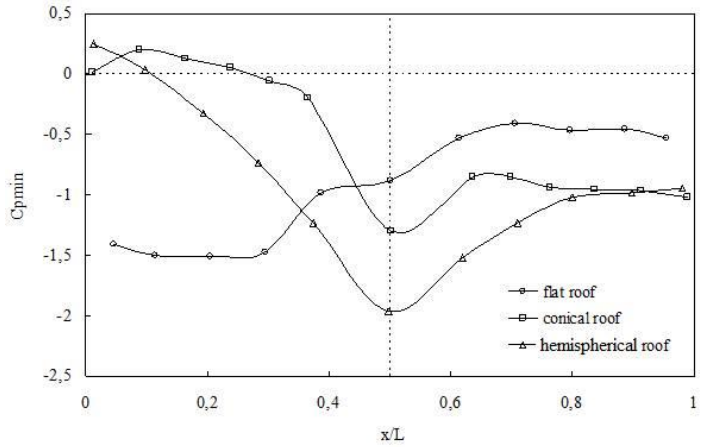

(b)

Fig. 13 Comparison of pressure distributions along the mid-axis of various roof geometries in the flow direction (a) mean (b) minimum

5. Conclusions

In this study, the effects of finite cylinder free end shape were investigated experimentally and numerically by using three different roof shapes: flat, conical and hemispherical. In the experimental part, mean, rms, maximum and minimum values of surface pressures on the roof and on the cylindrical wall were measured for three finite cylinder models having different roof shapes. In the numerical part, three dimensional flow fields around the same building models were computed by using Realizable k-ε turbulence model. Pressure distributions on the windward walls are positive due to impinging effect. Negative pressure fields occur both on the roof and leeward wall for the finite cylinder of flat roof. The largest negative pressures occur in separation flow region near the leading edge of the roof and are progressively reduced in magnitude in the reattachment region on the flat roof surface. There is symmetry of the pressures measured on the

roofs with respect to the windward meridian. For the conical roof, except the front part of the windward which is directly exposed to incoming flow, negative pressures were observed on the roof. More critical negative pressures are obtained on the roof regions perpendicular to the incoming flow because of the separated flow near the tip of the conical roof. For the hemispherical roof, similar to the conical roof, critical negative pressures occur on the roof regions normal to the incoming flow. The evaluation of pressure distributions on the three different roof shape shows that the largest negative pressure peak occurs on the top of hemispherical roof. Pressure distributions on both conical and hemispherical roofs have similar trend. Change in roof shapes causes significant differences on the pressure distributions. When compared the pressure distributions on roofs, it is seen that hemispherical roof has the most critical pressure field among the others. For all simulations, mean pressure coefficients computed Realizable k-ε turbulence model exhibit a good accordance with mean pressure coefficients obtained experimentally. It is noted that this turbulence model gives satisfactory results for prediction of these kinds of flow fields. It is hoped that this study would provide data for the further researches on this subject.

References

Afgan, I., Moulinec, C., Prosser, R. and Laurence, D. (2007), "Large eddy simulation of turbulent flow for wall-mounted cantilever cylinders of aspect ratio 6 and 10", *Int. J. Heat Fluid Fl.*, **28**, 561-574.

Blackmore, P.A., Tsorki, E. and Breeze, G. (2004), "Wind loads on cylindrical roofs", *COST Action C14 Impact of Wind and Storm on City Life and Built Environment*, von Karman Institute for Fluid Dynamics, D7.1-7.10.

Cheng, C.M. and Fu, C.L. (2010), "Characteristics of wind loads on a hemispherical dome in smooth flow and turbulent boundary layer", *J. Wind Eng. Ind. Aerod.*, **98**, 328-344.

Dobriloff, C. and Nitsche, W. (2009), "Surface pressure and wall shear stress measurements on a wall mounted cylinder", *Imaging Measurement Method NNFM*, 106.

Faghih, A.K. and Bahadori, M.N. (2010), "Three dimensional numerical investigation of air flow over domed roofs", *J. Wind Eng. Ind. Aerod.*, **98**, 161-168.

Farivar, D. (1981), "Turbulent uniform flow around cylinders of finite length", *AIAA J.*, **19**, 275-281.

Fröhlich, J. and Rodi, W. (2004), "LES of the flow around a circular cylinder of finite height", *Int. J. Heat Fluid Fl.*, **25**, 537-548.

Hain, R., Köhler, C.J. and Michaelis, D. (2008), "Tomographic and time resolved PIV measurements on a finite cylinder mounted on a flat plate", *Exp. Fluids*, **45** (4), 715-724.

Holman, J.P. (1994), "Experimental methods for engineer", *McGraw-Hill Book Company*, New York.

Hongo, T. (1995), "Experimental study of wind forces on spherical roofs", *Ph.D. Thesis*, Tohoku University.

Javadi, K. and Kinai, F. (2014), "On the turbulent flow structures over a short finite cylinders: numerical investigation", *Proceedings of the International Conference on Heat Transfer and Fluid Flow*, Prauge, August 11-12.

Kareem, A. and Cheng, C.M. (1999), "Pressure and force fluctuations on isolated roughened circular cylinders of finite length in boundary layer flows", *J. Fluid. Struct.*, **13**, 907-933.

Kitagawa, T., Fujino, Y., Kimura, K. and Mizuno, Y. (2002), "Wind pressures measurement on end-cell-induced vibration of a cantilevered circular cylinder", *J. Wind Eng. Ind. Aerod.*, **90**, 395-405.

Krajnovic, S. (2011), "Flow around a tall finite cylinder explored by large eddy simulation", *J. Fluid Mech.*, **676**, 294-317.

Leder, A. (2003), "3D-flow structures behind truncated circular cylinders", *Proceedings of the FEDSM'03, the 4th ASME/JSME joint fluids engineering conference*, Paper No: FEDSM2003-45083, Honolulu Hawaii.

Li, Y.Q., Tamura, Y., Yoshida, A., Katsumura, A. and Cho, K. (2006), "Wind loading and its effects on

single-layer reticulated cylindrical shells", *J. Wind Eng. Ind. Aerod.*, **94**, 949-973.
Macdonald, P.A., Kwok, K.C.S. and Holmes, J.H. (1988), "Wind loads on circular storage bins, silos and tanks: Point pressure measurements", *Research Report No. R529*, School of Civil and Mining Engineering University of Sydney, Australia.
Maher, F.J. (1966), "Wind loads on dome-cylinders and dome-cone shapes", *J. Struct. Div. - ASCE*, **91**(3), 79-96.
Mooneghi, M.A., Irwin, P. and Chowdhury, A.G. (2016), "Towards guidelines for design of loose-laid roof pavers for wind uplift", *Wind Struct.*, **22**(2), 133-160.
Okamoto, S. and Sunabashiri, Y. (1992), "Vortex shedding from a circular cylinder of finite length placed on a ground plane", *J. Fluid. Eng. - T ASME*, **114**, 512-521.
Park, C.W. and Lee, S.J. (2002), "Flow structure around a finite circular cylinder embedded in various atmospheric boundary layers", *Fluid Dynam. Res.*, **30**, 197-215.
Park, C.W. and Lee, S.J. (2003), "Flow structure around two finite circular cylinders located in boundary layer: side-by-side arrangement", *J. Fluid. Struct.*, **17**, 1043-1058.
Park, C.W. and Lee, S.J. (2004), "Effects of free-end corner shape on flow structure around a finite cylinder", *J. Fluid. Struct.*, **19**, 141-158.
Pattenden, R.J., Turnock, S.R. and Zhang, X. (2005), "Measurements of the flow over a low-aspect-ratio cylinder mounted on a ground plane", *Exp. Fluids*, **39**, 10-21.
Portela, G. and Godoy, L.A. (2005a), "Wind pressures and buckling of cylindrical steel tanks with a conical roof", *Journal of Constructional Steel Research*, **61**, 786-807.
Portela, G. and Godoy, L.A. (2005b), "Wind pressures and buckling of cylindrical steel tanks with a dome roof", *J. Constr. Steel Res.*, **61**, 808-824.
Purdy, D.M., Maher, P.E. and Frederick, D. (1967), "Model studies of wind loads on flat-top cylinders", *J. Struct. Div. - ASCE*, **93**, 379-395.
Sabransky, I.J. and Melbourne, W.H. (1987), "Design pressure distribution on circular silos with conical roofs", *J. Wind Eng. Ind. Aerod.*, **26**(1), 65-84.
Sumner, D. and Heseltine, J.L. (2008), "Tip vortex structure for a circular cylinder with a free end", *J. Wind Eng. Ind. Aerod.*, **96**, 1185-1196.
Tavakol, M.M., Yaghoibu, M. and Masoudi, M.M. (2010), "Air flow aerodynamic on a wall-mounted hemisphere for various turbulent boundary layers", *Exp. Therm. Fluid Sci.*, **34**, 538-553.
Taylor, T.J. (1991), "Wind pressures on a hemispherical dome", *J. Wind Eng. Ind. Aerod.*, **40**, 199-213.
Uematsu, Y., Moteki, T. and Hongo, T. (2008), "Model of wind pressure field on circular flat roofs and its application to load estimation", *J. Wind Eng. Ind. Aerod.*, **96**, 1003-1014.
Uematsu, Y., Watanabe, K., Sasaki, A., Yamada, M. and Hongo, T. (1999), "Wind-induced dynamic response and resultant load estimation of a circular flat roof", *J. Wind Eng. Ind. Aerod.*, **83**, 251-261.
Wang, Y. and Li, Q.S. (2015), "Wind pressure characteristics of a low-rise building with various openings on a roof corner", *Wind Struct.*, **21**(1), 1-23.
West, G.S. and Apelt, C.J. (1982), "The effects of tunnel blockage and aspect ratio on the mean flow past a circular cylinder with Reynolds numbers between 10^4 and 10^5", *J. Fluid Mech.*, **114**, 361-377.

CC